IOP Publishing Quantum Sci. Technol. 10 (2025) 015053 https://doi.org/10.1088/2058-9565/ad9ac7

Quantum Science and Technology

CrossMark

OPEN ACCESS

RECEIVED
24 June 2024

REVISED
16 October 2024

ACCEPTED FOR PUBLICATION
5 December 2024

PUBLISHED
23 December 2024

Original Content from this work may be used under the terms of the Creative Commons Attribution 4.0 licence.

Any further distribution of this work must maintain attribution to the author(s) and the title of the work, journal citation and DOI.

PAPER

Robust quantum metrology with random Majorana constellations

Aaron Z Goldberg[1], Jose R Hervas[2], Angel S Sanz[2], Andrei B Klimov[3], Jaroslav Řeháček[4], Zdeněk Hradil[4], Markus Hiekkamäki[5], Matias Eriksson[5], Robert Fickler[5], Gerd Leuchs[6] and Luis L Sánchez-Soto[6,*]

[1] National Research Council of Canada, 100 Sussex Drive, Ottawa, Ontario K1N 5A2, Canada
[2] Departamento de Óptica, Facultad de Física, Universidad Complutense, 28040 Madrid, Spain
[3] Departamento de Física, Universidad de Guadalajara, 44420 Guadalajara, Jalisco, Mexico
[4] Department of Optics, Palacký University, 17. listopadu 12, 771 46 Olomouc, Czech Republic
[5] Physics Unit, Photonics Laboratory, Tampere University, 33720 Tampere, Finland
[6] Max-Planck-Institut für die Physik des Lichts, 91058 Erlangen, Germany
[*] Author to whom any correspondence should be addressed.

E-mail: lsanchez@ucm.es

Keywords: Robust, quantum, metrology, Majorana, constellations

Supplementary material for this article is available online

Abstract

Even the most classical states are still governed by quantum theory. A number of physical systems can be described by their Majorana constellations of points on the surface of a sphere, where concentrated constellations and highly symmetric distributions correspond to the least and most quantum states, respectively. If these points are chosen randomly, how quantum will the resultant state be, on average? We explore this simple conceptual question in detail, investigating the quantum properties of the resulting random states. We find these states to be far from the norm, even in the large-number-of-particles limit, where classical intuition often replaces quantum properties, making random Majorana constellations peculiar and intriguing. Moreover, we study their usefulness in the context of rotation sensing and find numerical evidence of their robustness against dephasing and particle loss. We realize these states experimentally using light's orbital angular momentum degree of freedom and implement arbitrary unitaries with a multiplane light conversion setup to demonstrate the rotation sensing. Our findings open up new possibilities for quantum-enhanced metrology.

1. Introduction

Random matrices sampled from an ensemble with a specific symmetry were introduced by Wigner [1, 2] and Dyson [3–5] to describe spectral properties of quantum many-body systems, such as atomic nuclei [6]. Since then, random matrix theory [7–9] has found applications in fields as diverse as black holes [10–13] and gravity [14], quantum chaos [15], transport in disordered systems [16, 17], spin glasses [18], neural networks [19, 20], and even finance [21]. Quantum information is definitely one of the most recent applications, and a very natural one, too [22–24].

Random quantum states can be seen as arising from the time evolution of arbitrary initial states of quantum analogues of classically chaotic systems [25]. Furthermore, these states emerge when not much is known about a state and one wants to ask about its generic properties, characteristic of a 'typical' state [26–28]. Given a random quantum state, one may then ask how quantum is this state: does it exhibit classical behavior in the large-number-of-particles regime? If one had access to a black box that prepared random states, how much would it be worth and what would its applications be? These questions and more motivate the present study.

When considering the set of pure states living in an N-dimensional complex vector space, the manifold of physical states is the projective space $\mathbb{C}\mathbf{P}^N$ [29], wherein there is a unique normalized measure invariant under all unitary transformations: the associated Haar measure [30]. One can reasonably call this measure the uniform distribution over the unit sphere [31].

© 2024 The Author(s). Published by IOP Publishing Ltd

The geometrical properties of quantum states are essential to understanding where classical intuitions break down and where the next quantum advantage may lie [32–34]. In phase space, localization is a clear signature of the state quantumness [35, 36], as it has been demonstrated with several indicators, such as Rényi–Wehrl entropies [37], inverse participation ratio [38], or Husimi extrema [39]. However, while these notions provide effective analytical tools, the geometry of $\mathbb{C}\mathbf{P}^N$ is not very intuitive and so it is difficult to visualize and to gain insights into the nature of those states.

Here, we propose a novel class of random states based upon a mapping onto a many-qubit system (which, in some cases, might be fictitious). Actually, any system with a finite-dimensional Hilbert space of dimension $N = 2S + 1$ can be thought of as a spin S [40]. The space manifold $\mathbb{C}\mathbf{P}^N$ admits an appealing representation due to Majorana [41], which maps any pure state onto $2S$ points on the unit sphere $\mathcal{S}_2$; the state's stellar representation. This picture makes it natural to consider the states associated with random points on the sphere. We conduct a detailed study of these states from an SU(2)-invariant perspective. Notably, we find that, in the limit of a large number of particles, they do not converge to a classical state and preserve their quantumness.

In addition, these new random Majorana (RM) states belong to the symmetric (bosonic) subspace. It has been recognized that symmetric states offer significant advantages from a metrological perspective [42–45]. We find numerical evidence that the usefulness of RM states for rotation-sensing-style tasks, like magnetometry and ellipsometry, is robust against the loss of a finite number of particles and dephasing. This is in stark contrast to other relevant states, such as Greenberger–Horne–Zeilinger (GHZ) states [46] (equivalent to the NOON states [47] in optical interferometry), which completely lose their (otherwise ideal) sensitivity upon loss of just a single particle. Finally, we experimentally generate these states by utilizing light's orbital angular momentum and implement arbitrary unitaries using a multiplane light conversion setup to showcase rotation sensing.

This paper is organized as follows. In section 2 we address the basic notions of the Majorana stellar representation and its physical interpretation. In section 3 we raise the ideas behind RM constellations and characterize their properties by resorting to a multipole expansion. Subsequently, in section 4 we use these multipoles to compare our method with alternative ways of obtaining random states. In section 5 we introduce the setting of quantum parameter estimation. Utilizing the quantum Fisher information, we investigate the performance and robustness of the RM states under the influence of noise and particle loss. Finally, in section 6 we introduce the experimental setup used to study these states with respect to rotation sensing and analyze the obtained results. We conclude our work in section 7.

2. Majorana constellations

Let us consider a pure spin-S state $|\psi\rangle$ living in the $2S+1$-dimensional Hilbert space $\mathcal{H}_S$ spanned by the standard angular momentum basis $\{|S, m\rangle \mid m = -S, \ldots, S\}$, which is the carrier of the irreducible representation (irrep) of spin S of SU(2). This space is isomorphic to $\mathbb{C}^{2S+1}$, but since any two vectors in $\mathcal{H}_S$ differing by a phase represent the same physical state, the manifold of physical states is the projective space $\mathbb{C}\mathbf{P}^{2S}$ [29].

The merit of Majorana was to show that points in $\mathbb{C}\mathbf{P}^{2S}$ are in one-to-one correspondence with unordered sets of (possibly coincident) $2S$ points on the unit sphere $\mathcal{S}_2$. In other words, spin-S states can be obtained as fully symmetrized states of a system of $2S$ spins $1/2$ (or qubits). These systems have many physical applications, ranging from quantum computation to quantum sensing and metrology [48–52]. This idea is also at the heart of the Schwinger map [53, 54], which realizes the set of angular momentum operators in terms of polynomials of bosonic operators.

There are various ways to see why this is so, but probably the most direct one is to notice that the state $|\psi\rangle$ can always be written as

$$|\psi\rangle = \frac{1}{\mathcal{N}} \prod_{i=1}^{2S} a^\dagger_{-\mathbf{u}_i} |\mathrm{vac}\rangle, \tag{2.1}$$

where $\mathbf{u}_i$ is a unit direction of spherical coordinates (θ_i, ϕ_i), the rotated bosonic operators are

$$a^\dagger_{\mathbf{u}} = \cos(\theta/2)\, a^\dagger_+ + e^{i\phi} \sin(\theta/2)\, a^\dagger_- , \tag{2.2}$$

with $a^\dagger_+$ and $a^\dagger_-$ creating excitations in two modes (denoted by $+$ and $-$) from the two-mode vacuum $|\mathrm{vac}\rangle$, and $\mathcal{N}$ is a normalization factor of no interest for our purposes here and whose explicit expression can be found, e.g. in [55].

The set of $2S$ (non-necessarily distinct) unit vectors $\{\mathbf{u}_1, \ldots, \mathbf{u}_{2S}\}$ defines the Majorana constellation of the state. Alternatively, the state (2.1) can be expressed as

$$|\psi\rangle = P_\psi(a_+^\dagger, a_-^\dagger)|\text{vac}\rangle\,, \tag{2.3}$$

where $P_\psi(a_+^\dagger, a_-^\dagger)$ is a homogeneous polynomial of degree $2S$ in the variables $a_+^\dagger$ and $a_-^\dagger$ that can be factorized (up to an unessential factor) in the above form.

In particular, the states

$$|\mathbf{n}\rangle = \frac{1}{\sqrt{(2S)!}}\left(a_{\mathbf{n}}^\dagger\right)^{2S}|\text{vac}\rangle \tag{2.4}$$

are precisely the spin-S coherent states (CS) [56]. The definition shows that the associated constellations consist of only one single point in the antipodal direction $-\mathbf{n}$. It is natural to introduce the CS representation by $\psi(\mathbf{n}) \equiv \langle \mathbf{n}|\psi\rangle$: this is a *bona fide* wave function over the unit sphere $\mathcal{S}_2$. Simple algebraic manipulations yield

$$\psi(\mathbf{n}) = \prod_{i=1}^{2S}\left[\tfrac{1}{2}\left(1 - \mathbf{n}\cdot\mathbf{u}_i\right)\, \mathrm{e}^{i\Sigma(\mathbf{n},-\mathbf{u}_i)}\right], \tag{2.5}$$

where $\Sigma(\mathbf{n}, -\mathbf{u}_i)$ is the oriented area of the spherical triangle with vertices $(\mathbf{z}, \mathbf{n}, -\mathbf{u}_i)$, with $\mathbf{z}$ the unit vector in the direction of the axis Z. This confirms that the Majorana constellation consists of the zeros of $\psi(\mathbf{n})$.

The CS wavefunction induces a probability distribution

$$Q_\psi(\mathbf{n}) \equiv |\langle \mathbf{n}|\psi\rangle|^2\,, \tag{2.6}$$

which is the Husimi function [57], and whose zeros are also the Majorana constellation.

Because the Majorana representation facilitates a useful geometrical interpretation of quantum states, it has found an increasing number of applications in recent years, with prominent examples being polarimetry and magnetometry [58], Bose–Einstein condensates [59, 60], Berry phases [61–63], and studies of entanglement [64].

3. Random Majorana constellations

Since points on the sphere $\mathcal{S}_2$ correspond uniquely to pure states via the Majorana representation, one is immediately led to the simplest idea of how to generate RM states: they correspond to sets of random points on $\mathcal{S}_2$. Interestingly, the question of distributing points uniformly over a sphere has inspired substantial mathematical research [65–67], as has the question of random polynomials [68–71], in addition to attracting the attention of physicists working in a variety of fields.

We randomize each of the spherical coordinates (θ_i, ϕ_i) independently using the Haar measure $\sin\theta_i\, \mathrm{d}\theta_i\, \mathrm{d}\phi_i/4\pi$ for $\mathcal{S}_2$. Equivalently, the resulting RM states can be viewed as arising from the action of a random operator $U \in \mathrm{SU}(2)^{\otimes 2S}$ on the ground state of $2S$ qubits, followed by projection onto the symmetric subspace and normalization. This is fundamentally tied to the most robust deterministic technique for creating arbitrary bipartite states of light, which uses beam splitters and post selection to sequentially add a photon's coordinates on its Poincaré sphere as a new point to a state's existing Majorana constellation [72, 73]. When the states of the single photons are randomized, the resulting state immediately takes the form of equation (2.1) with random spherical coordinates. This basic scheme can then be used to create random states in the light's polarization degree of freedom for tasks like polarimetry.

The intrinsic SU(2) symmetry suggests using the germane notion of multipoles [74, 75] to characterize the resulting states. To this end, we expand the density matrix of the system as

$$\varrho = \sum_{K=0}^{2S}\sum_{q=-K}^{K} \varrho_{Kq} T_{Kq}\,, \tag{3.1}$$

where T_{Kq} are the spherical tensor operators, defined as [75]

$$T_{Kq} = \sqrt{\frac{2K+1}{2S+1}} \sum_{m,m'=-S}^{S} C_{Sm,Kq}^{Sm'} |S, m'\rangle\langle S, m|\,, \tag{3.2}$$

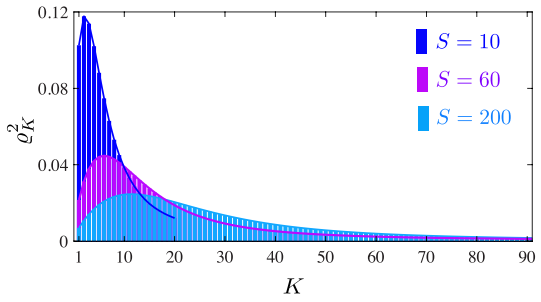

Figure 1. Mutipole distribution ϱ_K^2 for RM states with the values of S indicated in the inset.

with $C^{Sm'}_{Sm,Kq}$ being the Clebsch–Gordan coefficients that couple a spin S and a spin K ($0 \leqslant K \leqslant 2S$) to a total spin S. These tensors are an orthonormal basis

$$\mathrm{Tr}\left(T_{Kq}\, T^{\dagger}_{K'q'}\right) = \delta_{KK'}\delta_{qq'} \tag{3.3}$$

that transform appropriately under rotations $R(\mathbf{\Omega}) \in \mathrm{SU}(2)$:

$$R(\mathbf{\Omega})\; T_{Kq} R^{\dagger}(\mathbf{\Omega}) = \sum_p D^S_{pq}(\mathbf{\Omega})\; T_{Kp}\,, \tag{3.4}$$

where $D^S_{mn}(\mathbf{\Omega}) = \langle S, m|R(\mathbf{\Omega})|S, n\rangle$ are the usual Wigner D matrices [76].

The expansion coefficients are scalar values that are precisely the state multipoles. Alternatively, they can be computed as [48]

$$\varrho_{Kq} = \mathcal{C}_K \int_{\mathcal{S}_2} \mathrm{d}^2\mathbf{n}\; Q_\varrho(\mathbf{n})\;\; Y_{Kq}(\mathbf{n})\,, \tag{3.5}$$

where $\mathcal{C}_K$ is a constant, $Y_{Kq}(\mathbf{n})$ the standard spherical harmonics, and $\mathrm{d}^2\mathbf{n} = \sin\theta \mathrm{d}\theta\mathrm{d}\phi$ the invariant measure on $\mathcal{S}_2$. The multipoles thus appear as the standard ones in electrostatics, but replacing the charge density by $Q_\varrho(\mathbf{n})$ and distances by directions [77]. They are the Kth directional moments of the state and, therefore, they resolve progressively finer angular features with increasing K.

Since $Y_{Kq}(\mathbf{n})$ constitute an orthonormal basis on $\mathcal{S}_2$, we can immediately invert equation (3.5):

$$Q_\varrho(\mathbf{n}) = \mathcal{C}_K^{-1} \sum_{Kq} \varrho_{Kq} Y_{Kq}(\mathbf{n})\,, \tag{3.6}$$

so the multipoles represent the state's Q distribution on the sphere in its natural basis of spherical harmonics. As the Q function determines the Majorana constellation, these coefficients ϱ_{Kq} can also be directly computed from the constellation, as was recently explained in [78].

For each value of S, we average over 1.5×10^6 samples. In figure 1 we show the resulting multipoles plotted in terms of the multipole squared length

$$\varrho_K^2 = \sum_{q=-K}^{K} |\varrho_{Kq}|^2 \tag{3.7}$$

which are SU(2) invariant and thus serve as an effective tool for studying the states, treating all states related by an SU(2) transformation (a rigid rotation of the constellation) as equivalent. As we can see, only multipoles with small K contribute significantly. The maximally contributing multipole $K_{\max}$ smoothly increases with S: a least-squares fitting gives that, for large S, $K_{\max} = a\sqrt{S}$, with $a \simeq 0.8$.

To gain further insight into this behavior, in figure 2 we plot the average multipoles for RM states with $S = 60$. The broken lines delimit the corresponding variances, which are clearly not uniform. Since the individual multipole distributions are non-Gaussian, the variances give only partial information. To complete the picture, in the background we display a density plot representing the number of states with a given value of the Kth multipole. Notice that we use a logarithmic scale in order to better appreciate the behavior of higher Ks, which have exceedingly small values. We see the emergence of a striking multipeaked structure. The multipoles with significant yellow areas (i.e. a strong concentration of samples) are those with less variance.

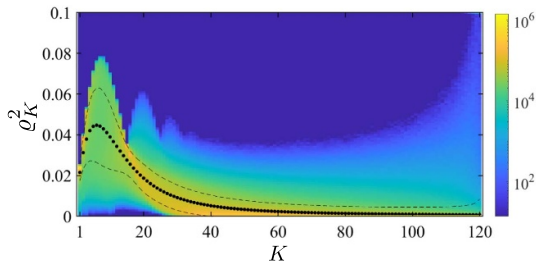

Figure 2. The dots represent the average multipoles for RM states with S 60. The broken lines delimit the associated variances. The density plot in the back (with the logarithmic scale shown at the right) is the number of trials having the corresponding value of the multipole.

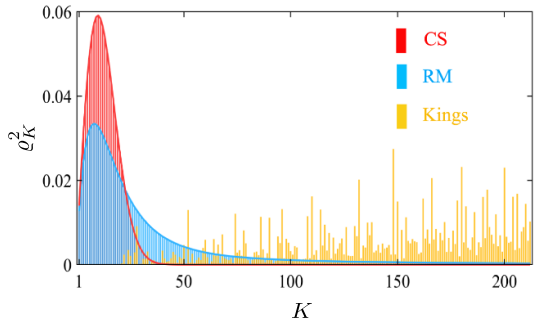

Figure 3. Multipole distribution for CS, RM, and Kings of Quantumness for $S = 106$. The colors in the inset indicate the corresponding states.

One sensible set of quantities in this scenario is the set of cumulative multipole distributions, defined as

$$A_M = \sum_{K=1}^{M} \varrho_K^2 . \tag{3.8}$$

Note that we ignore the 0th multipole as it corresponds only to normalization. For CS this quantity reaches the value

$$A_M^{\mathrm{CS}} = \frac{2S}{2S+1} - \frac{[\Gamma(2S+1)]^2}{\Gamma(2S-M)\,\Gamma(2S+M+2)} , \tag{3.9}$$

and it has been proven that this is indeed maximal for every $M \in \{1, \ldots, 2S\}$ [79]. At the opposite extreme we have states whose multipoles vanish up to the highest M: they have been dubbed as Kings of Quantumness [80] and they are maximally unpolarized. For each total spin S, there exists a maximal order M to which a state can be unpolarized; the state(s) satisfying this condition of $A_M = 0$ are the Kings. Therefore, A_M is a good measure of the quantum properties of a state through its *hidden polarization* features [81] that are stored in high-order multipoles.

To appreciate the different behaviors, in figure 3 we have plotted the multipole distributions for the most quantum (Kings of Quantumness), the least quantum (CS), and RM states for $S = 106$. The differences speak for themselves. A RM constellation is markedly different from a classical state: although the maximal contributions arise from roughly the same multipoles for both states (actually, for CS a quick estimate gives $K_{\max} \simeq \sqrt{S} - 1/2$), RM states have much heavier tails, thus hiding their quantum information in higher-order multipoles than CS. This makes them useful for metrological applications, even in the large-S limit, where quantum effects may be expected to vanish. Additionally, such RM states are far from the most quantum states, certifying the rarity of the Kings of Quantumness and the effort required for creating them. This behavior is confirmed by the cumulative multipole distribution A_M for the same states, as plotted in figure 4.

4. Comparison to other random distributions

If a pure state is expressed in the angular momentum basis as $|\psi\rangle = \sum_m \psi_m |S, m\rangle$, one could instead consider states with randomized probability amplitudes ψ_m. This can be achieved with a random unitary

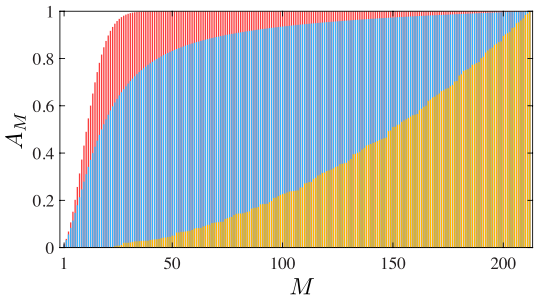

Figure 4. Cumulative multipole distribution for CS, RM, and Kings of Quantumness states for $S = 106$. The colors are the same as in figure 3.

$U \in \mathrm{SU}(2S+1)$ acting on the state, which is often called the circular unitary ensemble (CUE) [4]. These random unitaries were considered in [82] and [37], who found the Rényi–Wehrl entropies of the resulting random CUE states to be highly quantum. Moreover, in [45] it was demonstrated that such random CUE states are useful and robust for metrology.

Actually, we can calculate the expectation value of the cumulative multipole moments $\mathcal{A}_M = \int A_M \mathrm{d}U$ for a variety of normalized Haar measures $\mathrm{d}U$, through

$$\mathcal{A}_M = \sum_{K=1}^{M} \sum_{q=-K}^{K} \frac{2K+1}{2S+1} \sum_{m,m'=-S}^{S} C^{Sm+q}_{Sm,Kq} C^{Sm'+q}_{Sm',Kq} I_{m,m',q}, \tag{4.1}$$

with $I_{m,m',q} = \int \psi_{m+q} \psi^*_m \psi^*_{m'+q} \psi_{m'} \mathrm{d}U$, and $C^{Sm}_{S_1 m_1, S_2 m_2}$ the Clebsch–Gordan coefficients [76] that vanish unless the usual angular momentum coupling rules are satisfied: $m_1 + m_2 = m$, $0 \leqslant K \leqslant 2S$, and $-K \leqslant q \leqslant K$.

For example, if we express our random unitaries by $U \in \mathrm{SU}(2S+1)$, these integrals can be obtained exactly using random-matrix theory [83, 84] (see Supplemental Material). But there is another intuitive method: all of the nonzero integrals take the form $\int |\psi_m|^2 |\psi_n|^2 \mathrm{d}U$ and the distribution for each ψ_i is the same, so we know immediately that $I_{m,m',q} \propto \delta_{q,0} + \delta_{m,m'}$, such that

$$\mathcal{A}_{M,\,\mathrm{SU}(2S+1)} = \frac{M(M+2)}{(2S+1)(2S+2)}. \tag{4.2}$$

This means that states with random coefficients ψ_m have $\sum_{q=-K}^{K} |\varrho_{Kq}|^2 \propto 2K+1$, making them much more quantum than RM states and according with other results for this distribution [37, 82]. This is in stark contrast to the notion that both forms of randomness approach each other in the limit of large S in terms of the distance between arbitrary pairs of random states [85], stressing the differences maintained between the forms of randomness for all but $S = 1/2$.

Another possibility of obtaining a random spin-S state is to take a state of $2S$ random qubits. We employ the same procedure as used for the RM, beginning with the $2S$ qubits, but without normalizing the states initially. The resulting state is normalized at the end, ensuring that each state carries a weight proportional to its overlap with the symmetric subspace. This contrasts with the RM, where all states are assigned equal weight. This is not a unitary operation, instead creating the states from equation (2.1) with the replacement of the normalization constant by a state-independent factor $\mathcal{N} \to \sqrt{(2S)!}$, but it facilitates an analytical calculation whose cumbersome expression we show in the Supplemental Material.

Because each state in the ensemble has a different normalization due to having inhomogeneous likelihoods of being produced, the statistical properties derived for them should be understood as being weighted by the probabilities of finding the different projected states. These probabilities are proportional to $\mathcal{N}$ and their normalization can be found from the 0th order multipole. After normalizing the final results, we find that their multipolar distribution is very similar to that of CS. Intuitively, one can conclude that it is far more likely for such a projection method to produce a state close to CS than to produce a highly quantum state. The RM states may be thought of as states randomly chosen after the projection method succeeds, while the projected states are the result of randomization prior to the projection. In other words, if the RM can be thought of as a die with n equally likely sides, the projected states are the same die, but with each side having a different probability.

In figure 5 we display the conspicuous differences between the multipole distributions for these different randomized states.

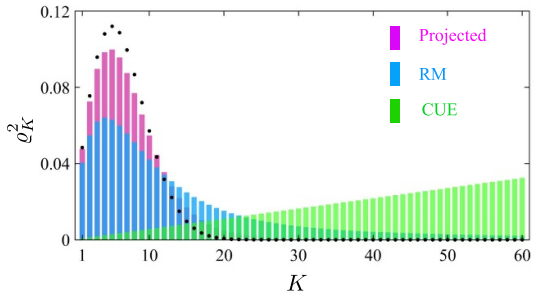

Figure 5. Multipole distribution for RM, CUE, and projected random qubits, all of them for $S = 30$. For comparison, the dots represent the multipoles for a CS.

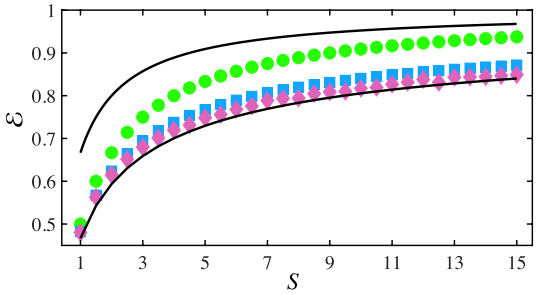

Figure 6. Quantumness $\mathcal{E}$ for the same random states considered in figure 5 as a function of S. The two continuous lines give the limit values of $\mathcal{E}$: the upper one is $2S/(2S+1)$, whereas the lower one corresponds to the CS.

The conclusion from the discussion thus far is that classical states convey their information in lower multipoles, whereas the opposite occurs for extremal quantum states. However, to assess this behavior in a quantitative way, we need a proper measure of quantumness. Since our analysis has been largely based on multipoles, we will use a recent proposal defined precisely in terms of them [86]; viz.,

$$\mathcal{E}(\varrho) = 1 - \sum_{K=0}^{2S} \frac{\varrho_K^2}{2K+1}\,. \tag{4.3}$$

$\mathcal{E}(\rho)$ takes an entanglement monotone for a particular decomposition of Hilbert space, the linear entropy of the pure state when decomposed over the modes $a_{\mathbf{u}}$ and $a_{-\mathbf{u}}$, then averages this over all possible two-mode decompositions that come from rotating the unit vector $\mathbf{u}$. We stress though that this metric is an entanglement monotone only for pure states. Equation (4.3) provides a mode-decomposition-agnostic measure of quantumness that is entanglement averaged over easy-to-perform entangling operations. Larger values of $\mathcal{E}$ signify more quantum states. This quantity emerges when looking at symmetric superpositions of two-mode states: it turns out that they can be entangled or separable, but this property can change after the Majorana constellation undergoes a rigid rotation. To properly account for this possibility, one can consider their linear entropy of entanglement averaged over all rotated partitions of the two-mode Hilbert space: the final result is precisely (4.3).

In figure 6 we calculate this measure for the different states discussed before for various values of S. We see that RM constellations are more quantum than states of random qubits projected onto the symmetric subspace, but less quantum than CUE states with random coefficients in the angular momentum basis. Impressively, the CUE states have $\mathcal{E}_{\rm CUE} = 2S/(2S+2)$ on average, which is very close to the maximum value for a single pure state: $2S/(2S+1)$. The lower continuous line in the figure corresponds to the values of $\mathcal{E}$ for CS, which are the least quantum ones.

This confirms the fact that the overwhelming majority of CUE random states are extremely close to the maximally entangled state [87] and that a significant portion of the RM states are entangled, which seems very counterintuitive. Moreover, we observe that for many functions defined over $\mathcal{H}_S$, the majority of vectors take a value of the function very close to the average value as $S \to \infty$. This observation, collectively, is referred to as the concentration of measure phenomenon [88].

5. Metrology with random states

We look next at the possibility of sensing rotations using random states. A general rotation is characterized by three parameters: the two angular coordinates fixing the rotation axis $\mathbf{u}(\Theta,\Phi)$ and the angle ω rotated around that axis [89]. In the space $\mathcal{H}_S$ the action of this rotation is represented by the operator [90]

$$R(\mathbf{\Omega}) = \exp(i\omega\,\mathbf{S}\cdot\mathbf{u})\,, \tag{5.1}$$

where we have used the notation $\mathbf{\Omega}(\omega,\mathbf{u}) = (\omega,\Theta,\Phi)$ to denote the three parameters and $\mathbf{S}$ is the vector comprising the three components of the angular momentum; the generators of the algebra $\mathfrak{su}(2)$.

The restriction of working in a single irrep is reasonable, since maximal precision will be obtained by concentrating all of the resources into a single subspace corresponding to the average total number of particles. This is true in the local regime, where prior information about the parameter in question is known [91], in sharp contrast to the global regime, where minimum error in estimating a completely unknown parameter requires coherences between irreps [92].

For the time being, we assume the rotation axis $\mathbf{u}$ to be known; the task is thus to estimate the rotation angle ω. A canonical scenario requires ω to be imprinted on a (preferably pure) probe state $|\psi\rangle$, in which the latter is shifted by applying a rotation $R(\omega)\in\mathrm{SU}(2)$ that encodes the angle ω. A set of measurements is then performed on the output state $|\psi_\omega\rangle = R(\omega)|\psi\rangle$, with the measurements represented by a positive operator-valued measure (POVM) [93] $\{\Pi_x\}$, where the POVM elements are labeled by an index x (discrete or continuous) that represents the possible outcomes of the measurement according to Born's rule $p(x|\omega) = \langle\psi_\omega|\Pi_x|\psi_\omega\rangle$. Afterward, what remains is to infer the angle via an estimator $\hat{\omega}$ [94], whose performance is usually assessed in terms of the variance. The ultimate limit for any possible POVM is given by the quantum Cramér–Rao bound (QCRB), which reads [33]

$$\mathrm{Var}_\psi(\hat{\omega}) \geqslant \frac{1}{\nu\,\mathsf{Q}_\psi(\omega)}\,, \tag{5.2}$$

where ν is the number of independent times the experiment is repeated. To assess the ultimate sensitivity per experimental trial, we take henceforth $\nu = 1$. Here, $\mathsf{Q}_\psi(\omega)$ is the quantum Fisher information (QFI), which depends exclusively on the initial probe state. We briefly recall that an explicit way to compute $\mathsf{Q}_\varrho(\omega)$ is as $\mathsf{Q}_\varrho(\omega) = \mathrm{Tr}(\varrho_\omega L_\omega^2)$ and L_ω is the so-called symmetric logarithmic derivative, defined implicitly via [95–97]

$$\frac{\partial\varrho_\omega}{\partial\theta} = \frac{1}{2}\{\varrho_\omega, L_\omega\}\,, \tag{5.3}$$

and $\{\cdot,\cdot\}$ stands for the anticommutator $\{A,B\} = AB + BA$. For pure initial states we have the simple result

$$\mathsf{Q}_\psi(\omega) = 4\,\mathrm{Var}_\psi(\mathbf{S}\cdot\mathbf{u})\,. \tag{5.4}$$

although generalizations to general density matrices are possible [98]. Convexity of the variance is responsible for a single irrep conferring maximal precision per number of particles. The QFI is thus maximal for pure states that maximize the variance of the generator $\mathbf{S}\cdot\mathbf{u}$: these are the states $|\mathbf{u}\rangle + |-\mathbf{u}\rangle)/\sqrt{2}$, which are the rotated versions of the time-honoured NOON states [47], defined as

$$|\mathrm{NOON}\rangle = \frac{1}{\sqrt{2}}\left(|S,S\rangle + |S,-S\rangle\right). \tag{5.5}$$

One may be interested in a probe state with the best average performance for any $\mathbf{u}$ rather than creating a distinct state for every axis. To this end, we consider the average QFI defined as

$$\bar{\mathsf{Q}}_\varrho(\omega) = \frac{1}{4\pi}\int_0^\pi \mathrm{d}\Theta\,\sin\Theta\int_0^{2\pi}\mathrm{d}\Phi\,\mathsf{Q}_\varrho(\omega)\,. \tag{5.6}$$

This average has been used in different issues of quantum information [99]. An exemplary context is magnetometry, where the magnitude of the magnetic field being sensed can be more important than its orientation. Then, $\bar{\mathsf{Q}}_\varrho(\omega)$ gives an upper bound on the attainable precision for a quantum state ϱ, if the direction of the magnetic field is chosen randomly based on a uniform distribution.

The maximum average QFI is achieved by states whose angular momentum projection vanishes in all directions; i.e.

$$\mathrm{Tr}(\varrho_\omega\mathbf{S}) = \mathbf{0}\,, \tag{5.7}$$

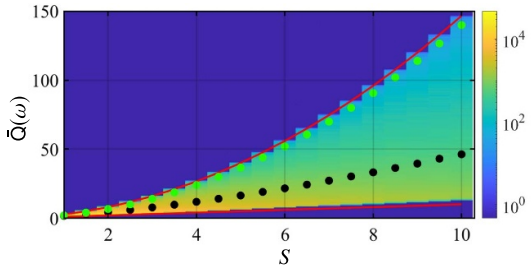

Figure 7. Average QFI as a function of the spin S. The black (green) dots denote the average value (over 60k trials) of the RM (CUE) states. The density plot in the back is the number of trials having the corresponding value of the average QFI for RM. The red lines indicate the maximum and minimum achiveable values of the QFI, corresponding to first-order unpolarized and CS, respectively.

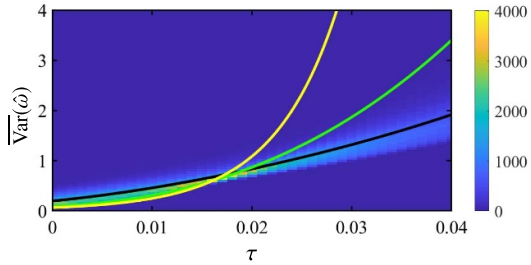

Figure 8. Average variance for RM (black line), CUE (green line) and King of Quantumness (yellow line) states as a function of the dimensionless time $\tau = \gamma t$ when the system experiences dephasing according to the model in equation (5.8). In all cases, $S = 3$. The density plot in the back is the same as in previous plots.

with a maximum value $\bar{\mathsf{Q}}_{\max} = \frac{4}{3}S(S+1)$. They correspond to first-order unpolarized states (which, among others, include the NOON states). In this sense, the most sensitive probe states are those whose classical angular momentum features are hidden [100, 101].

In figure 7 we plot the average $\bar{\mathsf{Q}}_{\varrho}(\omega)$ for both, RM and CUE states as a function of S. We also include the extremal values of this quantity, which are for first-order unpolarized and CS, respectively. The random states always lie in between these two lines, although CUE are closer to optimal. Some of the random states have QFI close to the maximum values, but most of them are concentrated below its average value.

In view of these results, one might wonder about the usefulness of random states. Intuition suggests that they should be more robust against imperfections than very fragile entangled states, as is the case for CUE states with certain types of loss [45]. To confirm this point, let us first consider the case of depolarization. We use the model devised in [102] for an SU(2)-invariant dephasing, which is appropriate for our case. The time evolution of the state is given by

$$\varrho(t) = \exp\left(-2\gamma t \mathbf{S}^2\right) \sum_{n=0}^{\infty} \sum_{j=x,y,z} \frac{(2\gamma t)^n}{n!} S_j^n \varrho(0) S_j^n \,, \tag{5.8}$$

where γ is a constant determining the strength of the dephasing, which we set to 1 without loss of generality. The results of the evolution under this dephasing are summarized in figure 8 for the case of $S = 3$, where we plot the minimum average variance of the angle estimator $\hat{\omega}$ as a function of the dimensionless time evolution (that can be easily converted to, e.g. traveled distance), for RM, CUE, and Kings of Quantumness states. The Kings are the optimal states to sense an arbitrary rotation when quantified by the highest QFI averaged over all rotations and by the lowest inverse QFI when averaged over all rotations [52], and, as expected, are very vulnerable to dephasing, and become much worse than the random, not only in their average values, but for most of their individual trials. Interestingly, RM are more robust than CUE and similar behavior is observed for other dimensions.

We next examine the case where a photon loss occurs. To analyze this scenario, we employ a simple SU(2)-invariant model that consists of mapping each state to an incoherent superposition of the states resulting from the removal of one particle, which in general is a mixed state in the space of spin $S - \frac{1}{2}$. In other words, we create $2S$ states by the removal of each one of the creation operators in equation (2.1) and add them incoherently, to explicitly look at random Majorana constellations that randomly lose a star; this is different from mode-agnostic removal of a particle [103] and is more in line with a preparation error where

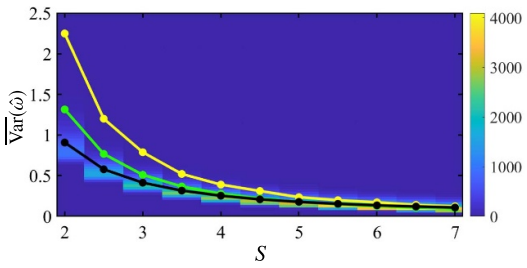

Figure 9. Average variance for RM (black line), CUE (green line) and King of Quantumness (yellow line) states as a function of S after losing one particle. The density plot in the back is the same as in previous plots.

one of the inputs is randomly neglected. The results are shown in figure 9, for the same states as in the previous figure. One can observe that for low S, random states exhibit again a clear advantage over Kings of Quantumness, albeit it diminishes as S increases.

The measurement saturating the QCRB has been characterized [52], but its experimental implementation may be challenging. Easier is to project the rotated state onto a set of coherent states for various directions and to reconstruct the rotation parameters from these measurements. Using the same basic principles applied to geographical positioning systems (GPS) [104], five projections are sufficient for this orientation problem, as has been recently demonstrated [105]. This is particularly useful in the context of random-state metrology, where we seek a single measurement scheme that is useful for all input states; while it cannot generally attain the averaged QFI, due to the QFI allowing for a different measurement for each term being averaged over, it can often perform very well, as demonstrated experimentally below.

6. Experimental results

The results of section 5 suggests that random states should perform well in rotation sensing tasks, in systems with imperfections. Hence, as a last step, we set out to test the suitability of random states for rotation sensing in the laboratory, where experimental imperfections can never be avoided. In these measurements, we used multiple different random states in the GPS-like measurement protocol mentioned above.

In our experimental implementation, we used the transverse-spatial degree of freedom of light. More specifically, we construct our Hilbert space $\mathcal{H}_S$ from a set of Laguerre–Gauss (LG) modes LG_ℓ^p, only choosing modes with a zero radial index $p=0$ and orbital angular momentum indices ℓ corresponding to the m index in the standard angular momentum basis $|S,m\rangle$. This is a standard system for probing SU(2) dynamics, even though it can also be analyzed with classical optics [107]. The beam radius was around 520 μm for the LG modes used to prepare the probe state. For both RM and CUE states, we follow the generation procedure described in sections 3 and 4, respectively, and translate the resulting states to our laboratory encoding using a set of $(2S+1)$ LG modes. We then constructed the rotation $R(\mathbf{\Omega})$, within this Hilbert space, using a multiplane light conversion (MPLC) device [108, 109]. For the measurements, Hilbert spaces with dimensions 5 and 7, corresponding to spins $S=2$ and $S=3$, respectively, were used.

The experimental setup is shown in figure 10 and can be divided into three distinct parts: probe state generation, unitary rotation of the probe state, and measurement of the rotated state. We used a CW laser at roughly 808.4 nm, for all of the measurements. The random probe states were created as coherent superpositions of the chosen set of LG modes by shaping an initial Gaussian field with an amplitude and phase modulating mask [110] on a spatial light modulator (SLM, Holoeye Pluto-2). An additional Gaussian correction was added to the masks [111, 112], and all of the SLMs used in the experiment had an added phase profile for aberration correction that was retrieved using the method introduced in [113].

In the second part of the experimental setup, an MPLC system, with five phase modulations, transforms the probe field according to the rotation transformation $R(\mathbf{\Omega})$. The phase modulations were performed on a single SLM, and each pair of consecutive modulations was separated by 800 mm of free-space propagation. The MPLC device is capable, in principle, of performing an arbitrary unitary mapping between spatial modes [108, 114].

A set of five phase modulating masks had to be designed, through a process called wavefront matching [115], for each of the 10 rotation angles $[(0, 36, \ldots, 324)$ degrees], in both the 5- and 7-dimensional systems. The rotation axis was kept fixed in each dimension. The third and final SLM was used to measure the rotated probe state by projecting it onto a transverse field structure [106].

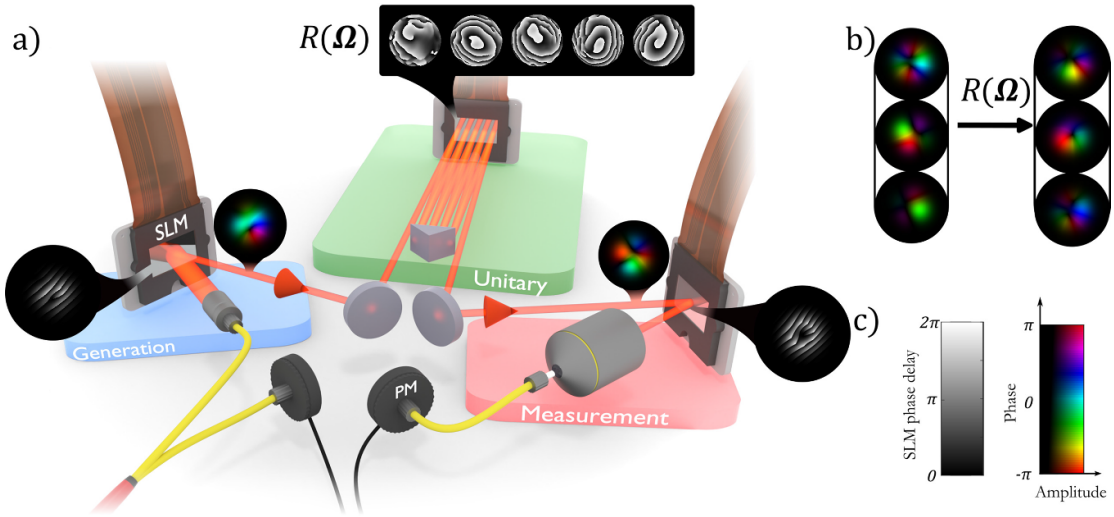

Figure 10. A simplified sketch of the experimental system is shown in (a). The initial laser output is split into two using a fiber beamsplitter with half of its power being directed onto a power meter (PM). The rest is collimated and sent onto the first of three SLMs. The Gaussian beam coming out of the single-mode fiber (SMF, yellow) is shaped into one of the chosen random states by the first SLM. The prepared probe state is then sent to the MPLC device that performs a unitary rotation operation $R(\mathbf{\Omega})$. After the MPLC, the rotated probe state is sent to the third SLM to be measured. The third SLM, together with a final single-mode fiber (SM), perform a projective measurement onto a state by first shaping the phase and amplitude of the beam and then coupling the first diffraction order of the SLM into the SMF using a 10 × microscope objective [106]. Non-magnifying 4*f* lens systems imaging each SLM onto the next one are omitted from the figure. The insets correspond to field structures (in color) and phase mask structures (in gray scale). Colorbars explaining the mode structure and gray-scale colormaps are given in (c). The holographic measurement mask shown in (a) filters for one of the chosen coherent states in the 5-dimensional Hilbert space. The field structure insets in (a) show an example of a state with a randomly distributed Majorana constellation for $S = 2$ and the same transverse field structure after the rotation unitary. In (b), more examples of states with random constellations are shown, along with their rotated counterparts. In the sketch of the experiment, the grating terms have been removed from the phase masks of the unitary and only the field structure at the first-diffraction orders from each phase mask are shown.

To perform the GPS-like measurement mentioned before, we probed each rotated random state $|\psi_{\mathbf{\Omega}}\rangle$ by projecting it onto a set of five coherent states, as described in detail in [105]. The explicit form of the FI matrix for this measurement is computed in [52]. Effectively, our measurements produced the quantities

$$\mathcal{Q}_{\mathbf{n}} = |\langle \mathbf{n}|\psi_{\mathbf{\Omega}}\rangle|^2 = \frac{P_{\langle \mathbf{n}|\psi_{\mathbf{\Omega}}\rangle}}{P_{\langle \psi_{\mathbf{\Omega}}|\psi_{\mathbf{\Omega}}\rangle}} \frac{\eta_{\psi_{\mathbf{\Omega}}}}{\eta_{\mathbf{n}}}, \tag{6.1}$$

where $P_{\langle \mathbf{n}|\psi_{\mathbf{\Omega}}\rangle}$ was the relative power coupled into the final SMF when projecting the rotated random state $|\psi_{\mathbf{\Omega}}\rangle$ onto the coherent state $|\mathbf{n}\rangle$, and $P_{\langle \psi_{\mathbf{\Omega}}|\psi_{\mathbf{\Omega}}\rangle}$ was the power coupled when projecting the rotated random state onto itself. The efficiencies $\eta_{\psi_{\mathbf{\Omega}}}$ and $\eta_{\mathbf{n}}$ are measured estimates of the state-dependent projection efficiencies: $\eta_{\psi_{\mathbf{\Omega}}}$ is the projection efficiency for the rotated random state measurement mask in question and similarly $\eta_{\mathbf{n}}$ is the efficiency of the CS projection.

The projection efficiencies were measured by first shaping the light field to the structure we want to project on in the generation, the MPLC was made to image the field structures, and the power of the field was measured both before the last SLM and after the last fiber. The efficiency was then estimated as the power after the fiber divided by the power before the measurement mask. The power measurements were normalized by dividing them with the power measured before the first spatial mode manipulation, as shown in figure 10. This was done to minimize the effects of changes in laser power throughout the measurements.

As mentioned before, the probe states used in the experiment were both RM and CUE states. In our specific experimental implementation, where transverse spatial modes are used to encode different types of random states, the primary challenge in preparing, modulating, and measuring the states with minimal errors arises from the increasing dimensionality of the state space. This difficulty stems from the increasingly intricate transverse phase and amplitude structures, coupled with the limited resolution of our devices. Consequently, all types of states can be considered equally challenging to work with, regardless of their specific nature.

However, since the difficulty of generating states will vary across different systems, it is essential to weight the ease of generating each type of state against its metrological power. Generally, we anticipate that the more entangled a state is on average, such as CUE or NOON states, the harder it will be to generate them accurately. This suggests that RM states may serve as a valuable and powerful alternative.

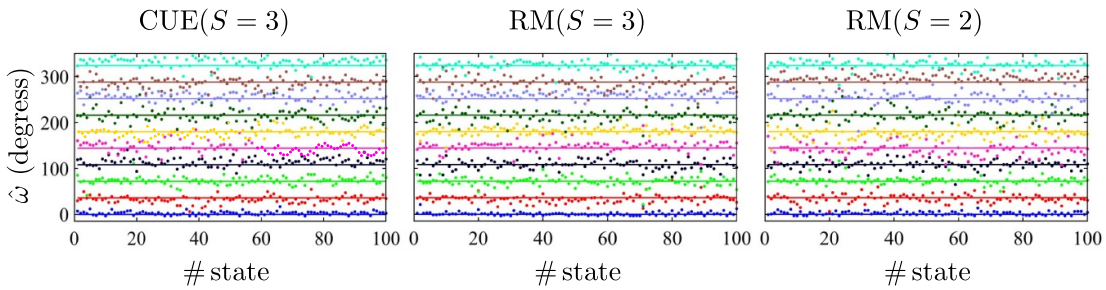

Figure 11. The dots are the estimated values of the rotation angle $\hat{\omega}$ for the CUE and RM states indicated in the upper labels. The horizontal axis labels the 100 random states used in each one of the experiments. The rotation axes used are given in equation (6.2). The true values of ω are $0, 36, \ldots, 324$ degrees and are indicated by horizontal lines.

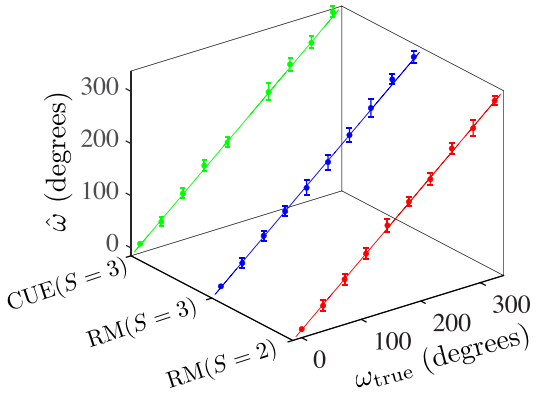

Figure 12. Statistics of the measurement for the states considered before in figure 11. The error bars represent standard deviations. The estimation procedure is local: the same states can be used for estimating a wide range of parameter values, but prior information about those parameters is essential to obtain the sensitivity limits dictated by local estimation theory.

It is important to stress that in our experimental setup there is no need to perform any projection onto the symmetric subspace, as the states are directly generated in $\mathcal{H}_S$. The concept of a symmetric subspace does not apply here, since our $\mathcal{H}_S$ does not originate from $2S$ qubits.

We performed the rotation measurement with 100 different random states of each type, with $\nu = 100$ repetitions of each relative-power measurement. The rotation axis $\mathbf{u}(\Theta, \Phi)$ was arbitrarily chosen for each value of S:

$$\mathbf{u}(\Theta,\Phi) = \begin{cases} \Theta = 34.9674^\circ, \Phi = 296.4448^\circ & S = 2, \\ \Theta = 157.948^\circ, \Phi = 137.361^\circ & S = 3\,. \end{cases} \tag{6.2}$$

Three different kinds of generalized maximum likelihood estimators were formed from this data set to verify the excellent rotational sensitivity of the fiducial states, following standard procedures [116, 117]. The estimator of the rotated angle ω reads

$$\hat{\omega} = \arg\max_{\omega} \sum_{j=1}^{5} \mathfrak{q}_j \log \frac{\mathcal{Q}_j}{\sum_{j'} \mathcal{Q}_{j'}}\,, \tag{6.3}$$

where $\mathfrak{q}_j$ is the measured value of $\mathcal{Q}_j = |\langle \mathbf{n}_j | \psi_{\mathbf{\Omega}} \rangle|^2$. This is equivalent to a quantum measurement where there are five meaningful outcomes, the measurement is repeated ν times, and the frequency with which each outcome occurs is proportional to $\mathfrak{q}_j$. The results appear in figure 11. The estimated values of ω show small fluctuations around the true values with very small typical standard deviations and negligible biases. The three cases look very similar.

To check the quality of our estimators, in figure 12 we have plotted the true values of ω versus the estimated ones. For each estimated point, we have included error bars determined by the corresponding standard deviation. The agreement emphasizes the excellent performance of the method. Moreover, figure 12 corroborates a unique property of random states: due to their typicality [118], they can unambigously

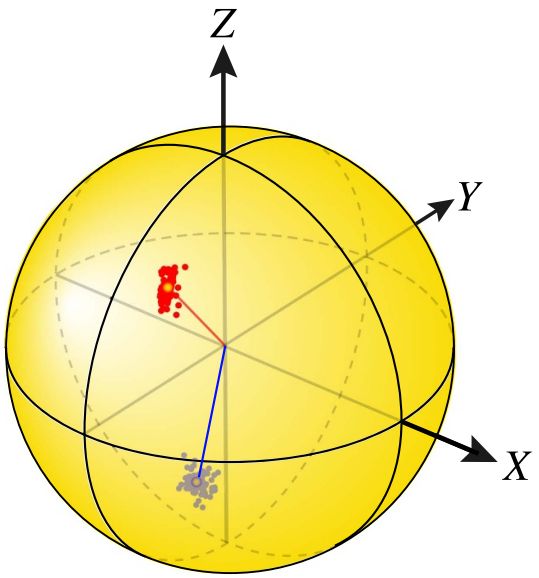

Figure 13. Estimated rotation axes for RM with $S=2$ (red points) and $S=3$ (blue points) using the data from figure 11.

estimate any rotation angle within a 2π range. This is in sharp contrast with other states such as NOON or of Quantumness that can distinguish angles within a range $\pi/(2S)$ [80].

Turning the assumptions around, we can take now the set of rotation angles as fixed, while assuming no prior knowledge of the rotation axis. The orientation of this axis can be estimated globally as follows

$$\hat{\mathbf{u}} = \arg\max_{\mathbf{u}} \sum_k \sum_j \mathfrak{q}_{jk} \log \frac{\mathcal{Q}_{jk}}{\sum_{k'} \sum_{j'} \mathcal{Q}_{k'j'}}, \tag{6.4}$$

where now $\mathcal{Q}_{jk} = |\langle \mathbf{n}_j | \psi_{k,\Omega} \rangle|^2$. This time, there is a bigger set of outcomes: each of the five quantum measurement outcomes for each of the rotation angles. Using this on the ensemble of 100 input RM states gives the statistics of inferred axis directions :

$$\hat{\mathbf{u}}(\hat{\Theta}, \hat{\Phi}) = \begin{cases} \hat{\Theta} = 35.31^\circ \pm 4.0^\circ, \hat{\Phi} = 295.8^\circ \pm 2.9^\circ & S = 2, \\ \hat{\Theta} = 138.4^\circ \pm 2.9^\circ, \hat{\Phi} = 157.2^\circ \pm 3.9^\circ & S = 3\,. \end{cases} \tag{6.5}$$

All the target true values are comfortably accommodated within those uncertainty regions. This estimation is nicely visualized on the sphere $\mathcal{S}_2$, as sketched in figure 13. The results for CUE random states are similar, although a bit less reliable due to experimental difficulties in getting the corresponding data.

These values can be compared with the best possible results respectively for the variances of $\hat{\Theta}$ and $\hat{\Phi}$ for a single measurement with a CS, which are (albeit for different orientations of CS)

$$\mathrm{Var}_{\mathrm{CS}}(\hat{\Theta}) = \mathrm{Var}_{\mathrm{CS}}(\hat{\Phi}) = \frac{1}{2S} \tag{6.6}$$

and the variances with Kings of Quantumness

$$\begin{aligned} \mathrm{Var}_{\mathrm{Kings}}(\hat{\Theta}) &= \frac{3}{16S(S+1)\sin^2(\omega/2)}, \\ \mathrm{Var}_{\mathrm{Kings}}(\hat{\Phi}) &= \frac{3}{16S(S+1)\sin^2(\omega/2)\sin^2\Theta}. \end{aligned} \tag{6.7}$$

When performing such a multiparameter estimation, the achievable uncertainties tend to depend on the actual values of the parameters. This dependence can be removed by choosing an appropriate weight matrix for combining the covariances of the different parameters: using the metric tensor for the group as the weight matrix allows all of the results to be independent from the parameter values and the chosen parametrization [119]. As in [105], such a figure of merit when estimating the angular coordinates of a unit vector is

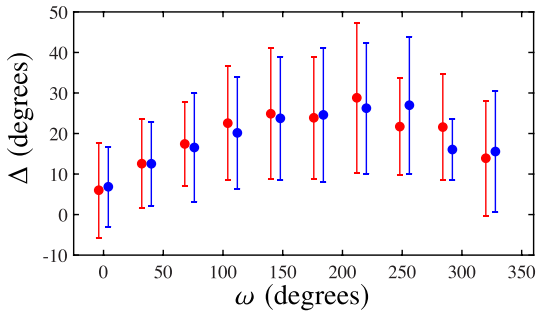

Figure 14. Deviation Δ between the true rotation and the estimated rotation for RM states with $S=2$ (red) and $S=3$ (blue), determined by the angle of rotation one would require to convert between the true and estimated rotation, as a function of the angle. The large error bars on the deviations make these results compatible with both quantum advantages (small deviations) and lack of demonstrated quantum advantages (large deviations); in all cases, the measurement method is demonstrated to be viable for determining all three parameters of a rotation.

$\Delta^2\hat{\Theta}+\sin^2\hat{\Theta}\Delta^2\hat{\Phi}$, here 0.00 488 634 and 0.00 257 369, as compared to the best possible values with a single coherent state of

$$\frac{1}{2S}\frac{2\cos\omega+\csc^2(\omega/2)+2}{2\sqrt{2}\sin\omega+\cos\omega+3}>\frac{0.3758}{2S}\,. \tag{6.8}$$

Finally, our detection scheme projecting onto five coherent states has a redundancy that makes possible to estimate simultaneously the axis of rotation and the angle of rotation. This implies maximizing the objective function

$$\{\hat{\omega},\hat{\mathbf{u}}\}=\arg\max_{\{\omega,\mathbf{u}\}}\sum_{j=1}^{5}\mathfrak{q}_j\log\frac{\mathcal{Q}_j}{\sum_{j'}\mathcal{Q}_{j'}}\,, \tag{6.9}$$

which requires global optimization tools [120]. Again, we are using a classical system to simulate a quantum measurement by taking the frequency of quantum measurement outcomes to be proportional to the relative power received for each of the five settings, then finding the variances of the maximum likelihood estimators that we take to be distributed according to the underlying probability distribution for the true parameters.

Errors of the inferred three parameters of the rotations can be quantified by considering the deviation Δ between the true rotation and the estimated rotation, determined by the angle of rotation one would require to convert between the true and estimated rotation, as $\Delta=\arg R(-\boldsymbol{\Omega})R(\hat{\boldsymbol{\Omega}})$, which can be found from the Hilbert-Schmidt norm as $\cos\Delta S+\sin\Delta S/\tan(\Delta/2)=\mathrm{Tr}[R(-\boldsymbol{\Omega})R(\hat{\boldsymbol{\Omega}})]$ [105]. This way, we find the average deviations

$$\Delta=\begin{cases}19.3^\circ\pm15.2^\circ & S=2\,,\\ 18.9^\circ\pm15.1^\circ & S=3\,.\end{cases} \tag{6.10}$$

The results are plotted for RM states in figure 14. These can be compared with the best possible results for measurement with a single CS as a probe state, which can never be used to estimate all three parameters of a rotation due to CS only depending on two coordinates that define the state's spin. Comparisons of schemes that split all of the trials into different subsets that each involve the same respective probe state can be found in the recent [121]. This allows us to conclude that the high rotational sensitivity of the RM states has been experimentally verified.

Although in our experiment the rotations have been artificially encoded using an MPLC system, the coherent-state projections used for the detection offer a range of advantages, including compactness, versatility, high efficiency, flexibility, and real-time adaptability. As already demonstrated in [105], this scheme is broad enough to apply to any other rotation-sensing application.

7. Concluding remarks

We have explored random Majorana constellations that arise as sets of points uniformly distributed on the sphere $\mathcal{S}_2$. The concept of state multipoles, intimately linked with the inherent SU(2) symmetry, has served as our main diagnostic tool to capture the amazing properties of these states. Additionally, these multipoles are sensible and experimentally-realizable quantities.

The family of symmetric states contains many metrologically useful states, including GHZ, NOON, and Dicke states, among others. However, all of them are extremely fragile resources. In contradistinction, random Majorana states, from their very same definition, are robust against imperfections such as dephasing and particle losses.

We have experimentally demonstrated the usefulness of these random constellations in protocols of quantum metrology. Apart from their incontestable geometrical beauty, there surely is plenty of room for the application of these states in a variety of physical contexts.

Data availability statement

All data that support the findings of this study are included within the article (and any supplementary files).

Acknowledgments

We are indebted to M Grassl, H Ferretti, A Steinberg, and K Życzkowski for discussions. This work was supported by the European Union's Horizon 2020 research and innovation programme under the QuantERA programme through the Project ApresSF. AZG acknowledges that the NRC headquarters is located on the traditional unceded territory of the Algonquin Anishinaabe and Mohawk people and support from NRC's Quantum Sensors Challenge Program and an NSERC Postdoctoral Fellowship. ABK acknowledges the Mexican CONAHCyT (Grant CBF2023-2024-50). MH acknowledges the Doctoral School of Tampere University, the Magnus Ehrnrooth Foundation, and the Emil Aaltonen Foundation. RF acknowledges support from the Academy of Finland through the Academy Research Fellowship (Decision 332399). ME, MH, RF acknowledge the support of the Academy of Finland through the Photonics Research and Innovation Flagship (PREIN-decision 320165). LLSS acknowledges support from Ministerio de Ciencia e Innovación (Grant PID2021-127781NB-I00).

ORCID iDs

Aaron Z Goldberg https://orcid.org/0000-0002-3301-7672
Jose R Hervas https://orcid.org/0000-0003-4499-7378
Angel S Sanz https://orcid.org/0000-0001-8617-5976
Andrei B Klimov https://orcid.org/0000-0001-8493-721X
Jaroslav Řeháček https://orcid.org/0000-0002-4969-2760
Zdeněk Hradil https://orcid.org/0000-0001-8732-4638
Markus Hiekkamäki https://orcid.org/0000-0002-3496-7338
Matias Eriksson https://orcid.org/0000-0002-3227-8037
Robert Fickler https://orcid.org/0000-0001-6251-753X
Gerd Leuchs https://orcid.org/0000-0003-1967-2766
Luis L Sánchez-Soto https://orcid.org/0000-0002-7441-8632

References

[1] Wigner E P 1955 Characteristic vectors of bordered matrices with infinite dimensions *Ann. Math.* **62** 548
[2] Wigner E P 1967 Random matrices in physics *Soc. Ind. Appl. Math. Rev.* **9** 1
[3] Dyson F J 1962 Statistical theory of the energy levels of complex systems. I *J. Math. Phys.* **3** 140
[4] Dyson F J 1962 Statistical theory of the energy levels of complex systems. II *J. Math. Phys.* **3** 157
[5] Dyson F J 1962 Statistical theory of the energy levels of complex systems. III *J. Math. Phys.* **3** 166
[6] Brody T A, Flores J, French J B, Mello P A, Pandey A and Wong S S M 1981 Random-matrix physics: spectrum and strength fluctuations *Rev. Mod. Phys.* **53** 385
[7] Mehta M L 2004 *Random Matrices* (Elsevier)
[8] Tao T 2012 *Topics in Random Matrix Theory* vol 132 (American Mathematical Society)
[9] Livan G, Novaes M and Vivo P 2018 *Introduction to Random Matrices: Theory and Practice* (Springer)
[10] Page D N 1993 Average entropy of a subsystem *Phys. Rev. Lett.* **71** 1291
[11] Page D N 1993 Information in black hole radiation *Phys. Rev. Lett.* **71** 3743
[12] Sen S 1996 Average entropy of a quantum subsystem *Phys. Rev. Lett.* **77** 1
[13] Renner R and Wang J The black hole information puzzle and the quantum de Finetti theorem 2021 (arXiv:2110.14653 [hep-th])
[14] Francesco P D, Ginsparg P and Zinn-Justin J 1995 2D gravity and random matrices *Phys. Rep.* **254** 1
[15] Bohigas O, Giannoni M J and Schmit C 1984 Characterization of chaotic quantum spectra and universality of level fluctuation laws *Phys. Rev. Lett.* **52** 1
[16] Mello P A 1990 Averages on the unitary group and applications to the problem of disordered conductors *J. Phys. A: Math. Gen.* **23** 4061
[17] Beenakker C W J 1997 Random-matrix theory of quantum transport *Rev. Mod. Phys.* **69** 731
[18] Cugliandolo L F, Kurchan J, Parisi G and Ritort F 1995 Matrix models as solvable glass models *Phys. Rev. Lett.* **74** 1012
[19] Sompolinsky H, Crisanti A and Sommers H J 1988 Chaos in random neural networks *Phys. Rev. Lett.* **61** 259

[20] Wainrib G and Touboul J 2013 Topological and dynamical complexity of random neural networks *Phys. Rev. Lett.* **110** 118101
[21] Bouchaud J and Potters M 2000 *Theory of Finance Risks: From Statistical Physics to Risk Management* (Cambridge University Press)
[22] Collins B and Nechita I 2015 Random matrix techniques in quantum information theory *J. Math. Phys.* **57** 015215
[23] Russell N J, Chakhmakhchyan L, O'Brien J L and Laing A 2017 Direct dialling of Haar random unitary matrices *New J. Phys.* **19** 033007
[24] Boixo S, Isakov S V, Smelyanskiy V N, Babbush R, Ding N, Jiang Z, Bremner M J, Martinis J M and Neven H 2018 Characterizing quantum supremacy in near-term devices *Nat. Phys.* **14** 595
[25] Haake F 1991 *Quantum Signatures of Chaos* (Springer)
[26] Wootters W K 1990 Random quantum states *Found. Phys.* **20** 1365
[27] Hayden P, Leung D, Shor P W and Winter A 2004 Randomizing quantum states: constructions and applications *Commun. Math. Phys.* **250** 371
[28] Życzkowski K, Penson K A, Nechita I and Collins B 2011 Generating random density matrices *J. Math. Phys.* **52** 062201
[29] Bengtsson I and Życzkowski K 2017 *Geometry of Quantum States: an Introduction to Quantum Entanglement* (Cambridge University Press)
[30] Alfsen E M 1963 A simplified constructive proof of the existence and uniqueness of Haar measure *Math. Scand.* **12** 106
[31] Życzkowski K and Kuś M 1994 Random unitary matrices *J. Phys. A: Math. Gen.* **27** 4235
[32] Mielnik B 1968 Geometry of quantum states *Commun. Math. Phys.* **9** 55
[33] Braunstein S L and Caves C M 1994 Statistical distance and the geometry of quantum states *Phys. Rev. Lett.* **72** 3439
[34] Nielsen M A, Dowling M R, Gu M and Doherty A C 2006 Quantum computation as geometry *Science* **311** 1133
[35] Goldberg A Z, Klimov A B, Grassl M, Leuchs G and Sánchez-Soto L L 2020 Extremal quantum states *AVS Quantum Sci.* **2** 044701
[36] Rudziński M, Burchardt A and Życzkowski K 2024 Orthonormal bases of extreme quantumness *Quantum* **8** 1234
[37] Gnutzmann S and Życzkowski K 2001 Rényi-Wehrl entropies as measures of localization in phase space *J. Phys. A: Math. Gen.* **34** 10123
[38] Wobst A, Ingold G-L, Hänggi P and Weinmann D 2003 Phase-space signatures of the Anderson transition *Phys. Rev.* B **68** 085103
[39] Marian P and Marian T A 2020 A geometric measure of non-classicality *Phys. Scr.* **95** 054005
[40] Ganczarek W, Kuś M and Życzkowski K 2012 Barycentric measure of quantum entanglement *Phys. Rev.* A **85** 032314
[41] Majorana E 1932 Atomi orientati in campo magnetico variabile *Nuovo Cimento* **9** 43
[42] Hyllus P, Gühne O and Smerzi A 2010 Not all pure entangled states are useful for sub-shot-noise interferometry *Phys. Rev.* A **82** 012337
[43] Benatti F and Braun D 2013 Sub–shot-noise sensitivities without entanglement *Phys. Rev.* A **87** 012340
[44] Apellaniz I, Lücke B, Peise J, Klempt C and Tóth G 2015 Detecting metrologically useful entanglement in the vicinity of Dicke states *New J. Phys.* **17** 083027
[45] Oszmaniec M, Augusiak R, Gogolin C, Kołodyński J, Acín A and Lewenstein M 2016 Random bosonic states for robust quantum metrology *Phys. Rev.* X **6** 041044
[46] Greenberger D M, Horne M A and Zeilinger A 1989 *Going Beyond Bell's Theorem* (Springer) pp 69–72
[47] Dowling J P 2008 Quantum optical metrology–the lowdown on high-N00N states *Contemp. Phys.* **49** 125
[48] Bouchard F *et al* 2017 Quantum metrology at the limit with extremal Majorana constellations *Optica* **4** 1429
[49] Chryssomalakos C and Hernández-Coronado H 2017 Optimal quantum rotosensors *Phys. Rev.* A **95** 052125
[50] Goldberg A Z and James D F V 2018 Quantum-limited Euler angle measurements using anticoherent states *Phys. Rev.* A **98** 032113
[51] Martin J, Weigert S and Giraud O 2020 Optimal detection of rotations about unknown axes by coherent and anticoherent states *Quantum* **4** 285
[52] Goldberg A Z, Klimov A B, Leuchs G and Sánchez-Soto L L 2021 Rotation sensing at the ultimate limit *J. Phys: Photon.* **3** 022008
[53] Schwinger J 1965 On angular momentum *Quantum Theory of Angular Momentum* ed L C Biedenharn and H Dam (Academic)
[54] Chaturvedi S, Marmo G, Mukunda N, SIMON R and ZAMPINI A 2006 The Schwinger representation of a group: concept and applications *Rev. Math. Phys.* **18** 887
[55] Liu H D and Fu L B 2014 Representation of Berry phase by the trajectories of Majorana stars *Phys. Rev. Lett.* **113** 240403
[56] Perelomov A 1986 *Generalized Coherent States and Their Applications* (Springer)
[57] Husimi K 1940 Some formal properties of the density matrix *Proc. Phys. Math. Soc. Japan* **22** 264
[58] Goldberg A Z 2019 Quantum theory of polarimetry: from quantum operations to Mueller matrices *Phys. Rev. Res.* **2** 023038
[59] Lian B, Ho T-L and Zhai H 2012 Searching for non-Abelian phases in the Bose-Einstein condensate of dysprosium *Phys. Rev.* A **85** 051606
[60] Cui X, Lian B, Ho T-L, Lev B L and Zhai H 2013 Synthetic gauge field with highly magnetic lanthanide atoms *Phys. Rev.* A **88** 011601
[61] Hannay J H 1998 The Majorana representation of polarization and the Berry phase of light *J. Mod. Opt.* **45** 1001
[62] Hannay J H 1998 The Berry phase for spin in the Majorana representation *J. Phys. A: Math. Gen.* **31** L53
[63] Bruno P 2012 Quantum geometric phase in Majorana's stellar representation: mapping onto a many-body Aharonov-Bohm phase *Phys. Rev. Lett.* **108** 240402
[64] Liu H D and Fu L B 2016 Berry phase and quantum entanglement in Majorana's stellar representation *Phys. Rev.* A **94** 022123
[65] Saff E B and Kuijlaars A B J 1997 Distributing many points on a sphere *Math. Intell.* **19** 5
[66] Brauchart J S and Grabner P J 2015 Distributing many points on spheres: minimal energy and designs *J. Complexity* **31** 293
[67] Alishahi K and Zamani M 2015 The spherical ensemble and uniform distribution of points on the sphere *Electron. J. Probab.* **20** 1
[68] Bharucha-Reid A T and Sambandham M 1986 *Random Polynomials* (Academic)
[69] Hannay J H 1996 Chaotic analytic zero points: exact statistics for those of a random spin state *J. Phys. A: Math. Gen.* **29** L101
[70] Prosen T 1996 Exact statistics of complex zeros for Gaussian random polynomials with real coefficients *J. Phys. A: Math. Gen.* **29** 4417
[71] Bogomolny E, Bohigas O and Leboeuf P 1996 Quantum chaotic dynamics and random polynomials *J. Stat. Phys.* **85** 639
[72] Fiurasek J 2002 Conditional generation of *n*-photon entangled states of light *Phys. Rev.* A **65** 053818
[73] Kok P, Lee H and Dowling J P 2002 Creation of large-photon-number path entanglement conditioned on photodetection *Phys. Rev.* A **65** 052104
[74] Fano U and Racah G 1959 *Irreducible Tensorial Sets* (Academic)
[75] Blum K 1981 *Density Matrix Theory and Applications* (Plenum)
[76] Varshalovich D A, Moskalev A N and Khersonski V K 1988 *Quantum Theory of Angular Momentum* (World Scientific)
[77] Jackson J D 1999 *Classical Electrodynamics* 3rd edn (Wiley)

[78] Romero J L, Klimov A B, Goldberg A Z, Leuchs G and Sánchez-Soto L L 2024 Multipoles from Majorana constellations *Phys. Rev.* A **109** 012214
[79] Björk G, Klimov A B, de la Hoz P, Grassl M, Leuchs G and Sánchez-Soto L L 2015 Extremal quantum states and their Majorana constellations *Phys. Rev.* A **92** 031801
[80] Björk G, Grassl M, de la Hoz P, Leuchs G and Sánchez-Soto L L 2015 Stars of the quantum Universe: extremal constellations on the Poincaré sphere *Phys. Scr.* **90** 108008
[81] Klyshko D 1992 Multiphoton interference and polarization effects *Phys. Lett.* A **163** 349
[82] Słomczyński W and Życzkowski K 1998 Mean dynamical entropy of quantum maps on the sphere diverges in the semiclassical limit *Phys. Rev. Lett.* **80** 1880
[83] Weingarten D 1978 Asymptotic behavior of group integrals in the limit of infinite rank *J. Math. Phys.* **19** 999
[84] Gorin T and López G V 2008 Monomial integrals on the classical groups *J. Math. Phys.* **49** 013503
[85] Życzkowski K and Slomczynski W 2001 The Monge metric on the sphere and geometry of quantum states *J. Phys. A: Math. Gen.* **34** 6689
[86] Goldberg A Z, Grassl M, Leuchs G and Sánchez-Soto L L 2021 Quantumness beyond entanglement: the case of symmetric states *Phys. Rev.* A **105** 022433
[87] Hayden P, Leung D W and Winter A 2006 Aspects of generic entanglement *Commun. Math. Phys.* **265** 95
[88] Singh U, Zhang L and Pati A K 2016 Average coherence and its typicality for random pure states *Phys. Rev.* A **93** 032125
[89] Grafarend E W and Kühnel W 2011 A minimal atlas for the rotation group so(3) *Int. J. Geomath.* **2** 113
[90] Cornwell J F 1984 *Group Theory in Physics* vol II (Academic)
[91] Kolenderski P and Demkowicz-Dobrzanski R 2008 Optimal state for keeping reference frames aligned and the platonic solids *Phys. Rev.* A **78** 052333
[92] Chiribella G, D'Ariano G M, Perinotti P and Sacchi M F 2004 Efficient use of quantum resources for the transmission of a reference frame *Phys. Rev. Lett.* **93** 180503
[93] Helstrom C W 1976 *Quantum Detection and Estimation Theory* (Academic)
[94] Kay S M 1993 *Fundamentals of Statistical Signal Processing* vol 1 (Prentice Hall)
[95] Szczykulska M, Baumgratz T and Datta A 2016 Multi-parameter quantum metrology *Adv. Phys.* X **1** 621
[96] Sidhu J S and Kok P 2020 Geometric perspective on quantum parameter estimation *AVS Quantum Sci.* **2** 014701
[97] Albarelli F, Barbieri M, Genoni M G and Gianani I 2020 A perspective on multiparameter quantum metrology: from theoretical tools to applications in quantum imaging *Phys. Lett.* A **384** 126311
[98] Fiderer L J, Fraïsse J M E and Braun D 2019 Maximal quantum Fisher information for mixed states *Phys. Rev. Lett.* **123** 250502
[99] Tóth G and Apellaniz I 2014 Quantum metrology from a quantum information science perspective *J. Phys. A: Math. Theor.* **47** 424006
[100] Goldberg A Z, de la Hoz P, Björk G, Klimov A B, Grassl M, Leuchs G and Sánchez-Soto L L 2020 Quantum concepts in optical polarization *Adv. Opt. Photon.* **13** 1
[101] Serrano-Ensástiga E, Chryssomalakos C and Martin J 2024 Quantum metrology of rotations with mixed spin states (arXiv:2404.15548)
[102] Rivas A and Luis A 2013 SU(2)-invariant depolarization of quantum states of light *Phys. Rev.* A **88** 052120
[103] Goldberg A Z 2024 Correlations for subsets of particles in symmetric states: what photons are doing within a beam of light when the rest are ignored *Opt. Quantum* **2** 14
[104] Hofmann-Wellenhof B, Lichtenegger H and Collins J 2001 *Global Positioning System* (Springer)
[105] Eriksson M, Goldberg A Z, Hiekkamäki M, Bouchard F, Rehacek J, Hradil Z, Leuchs G, Fickler R and Sánchez-Soto L L 2023 Sensing rotations with multiplane light conversion *Phys. Rev. Appl.* **20** 024052
[106] Bouchard F, Valencia N H, Brandt F, Fickler R, Huber M and Malik M 2018 Measuring azimuthal and radial modes of photons *Opt. Express* **26** 31925
[107] D'Ambrosio V, Spagnolo N, Del Re L, Slussarenko S, Li Y, Kwek L C, Marrucci L, Walborn S P, Aolita L and Sciarrino F 2013 Photonic polarization gears for ultra-sensitive angular measurements *Nat. Commun.* **4** 2432
[108] Morizur J F, Nicholls L, Jian P, Armstrong S, Treps N, Hage B, Hsu M, Bowen W, Janousek J and Bachor H-A 2010 Programmable unitary spatial mode manipulation *J. Opt. Soc. Am.* A **27** 2524
[109] Labroille G, Denolle B, Jian P, Genevaux P, Treps N and Morizur J-F 2014 Efficient and mode selective spatial mode multiplexer based on multi-plane light conversion *Opt. Express* **22** 15599
[110] Bolduc E, Bent N, Santamato E, Karimi E and Boyd R W 2013 Exact solution to simultaneous intensity and phase encryption with a single phase-only hologram *Opt. Lett.* **38** 3546
[111] Plachta S Z D, Hiekkamäki M, Yakaryılmaz A and Fickler R 2022 Quantum advantage using high-dimensional twisted photons as quantum finite automata *Quantum* **6** 752
[112] Hiekkamäki M, Barros R F, Ornigotti M and Fickler R 2022 Observation of the quantum Gouy phase *Nat. Photon.* **16** 1
[113] Jesacher A, Schwaighofer A, Fürhapter S, Maurer C, Bernet S and Ritsch-Marte M 2007 Wavefront correction of spatial light modulators using an optical vortex image *Opt. Express* **15** 5801
[114] Brandt F, Hiekkamäki M, Bouchard F, Huber M and Fickler R 2020 High-dimensional quantum gates using full-field spatial modes of photons *Optica* **7** 98
[115] Fontaine N K, Ryf R, Chen H, Neilson D T, Kim K and Carpenter J 2019 Laguerre-Gaussian mode sorter *Nat. Commun.* **10** 1
[116] Hradil Z, Mogilevtsev D and Řeháček J 2006 Biased tomography schemes: an objective approach *Phys. Rev. Lett.* **96** 230401
[117] Řeháček J, Mogilevtsev D and Hradil Z 2008 Tomography for quantum diagnostics *New J. Phys.* **10** 043022
[118] Garnerone S, de Oliveira T R and Zanardi P 2010 Typicality in random matrix product states *Phys. Rev.* A **81** 032336
[119] Goldberg A Z, Sánchez-Soto L L and Ferretti H 2021 Intrinsic sensitivity limits for multiparameter quantum metrology *Phys. Rev. Lett.* **127** 110501
[120] Horst R and Pardalos P M 1995 *Handbook of Global Optimization* (Springer)
[121] Ferretti H, Batuhan Yilmaz Y, Bonsma-Fisher K, Goldberg A Z, Lupu-Gladstein N, Pang A O T, Rozema L A and Steinberg A M 2024 Generating a 4-photon tetrahedron state: toward simultaneous super-sensitivity to non-commuting rotations *Opt. Quantum* **2** 91